

NLoS underwater VLC system performance: static and dynamic channel modeling

ABD EL-RAHMAN A. EL-FIKKY,¹ MARAM ESSAM ELDIN,¹ HEBA A. FAYED,¹
AHMED ABD EL AZIZ,¹ HOSSAM M. H. SHALABY,^{2,3}  AND MOUSTAFA H. ALY^{1,*} 

¹College of Engineering and Technology, Arab Academy for Science, Technology and Maritime Transport, Alexandria 1029, Egypt

²Electrical Engineering Department, Alexandria University, Alexandria 21544, Egypt

³Department of Electronics and Communications Engineering, Egypt-Japan University of Science and Technology E-JUST, Alexandria 21934, Egypt

*Corresponding author: mosaly@aast.edu

Received 6 August 2019; revised 17 September 2019; accepted 23 September 2019; posted 24 September 2019 (Doc. ID 374658); published 18 October 2019

In this paper, the impact of water channels under different communication link parameters is studied for underwater visible light communication (UVLC). The objective is to highlight the best results for non-line of sight (NLoS) communication links. In addition, NLoS links are studied under different parameters: LED colors, viewing angle, receiving angle, and data rates. The results are obtained and plotted using MATLAB simulation. The performance of the received power is first measured at different wavelengths and data rates. Then, the best results are further investigated at different viewing angles and receiving angles. The obtained results show that using cyan color provides more depth for the NLoS case, as well as a low bit error rate compared to the other colors. Most of the literature is concerned with unpractical configurations in underwater scenarios, such as an empty sea or assuming no human-object or blockage environment. We use the practical setup in Zemax Optics Studio to allow a precise description of ray tracing and high order of reflections inside a sea water environment. The channel impulse response (CIR) is obtained for static channel modeling, including a blockage environment to evaluate the best transmitters in sea water. Also, we are able to compare the average delay and the average delay spread of the source colors. The reflection characteristics of the sea water are considered as wavelength dependent. The CIR obtained by Zemax Solver and MATLAB indicates that cyan is the best source in sea water for different LED chips. Moreover, other previous studies assume perfect alignment scenarios between divers, which is not practical and not suitable for real channel gain results. Accordingly, we present a comprehensive dynamic channel modeling and characterization study for UVLC. Our study is based on Zemax programming language (ZPL) combined with Zemax Optics Studio. Using ZPL enables us to apply a mobility algorithm for divers and measure the channel gain variations due to random motion. We introduce a dynamic motion in a single-input single-output scenario and a single-input multiple-output scenario in the presence of blockage divers. Statistical analyses are studied for the appropriate distributions that can fit the data with various transmitter and receiver specifications. All dynamic scenarios are performed using cyan color in sea water, as it is proven to have satisfactory performance. The statistical results are beneficial for further analysis. As case studies, we consider various underwater scenarios, and the resulting parameters of statistical distributions can be used for future analysis in UVLC dynamic environments. © 2019 Optical Society of America

<https://doi.org/10.1364/AO.58.008272>

1. INTRODUCTION

Underwater wireless communication is a hot topic today. Wireless sensor networks, however, are highly distorted and attenuated in an underwater environment. Acoustic systems provide adequate underwater communications due to the proper sound propagation in water channels, although their maximum allowable data rate approaches ~ 10 kbps. Among

the drawbacks of optical fiber links are maintenance and installation costs. Moreover, the lack of optical fiber mobility is a major problem in many applications. Other limitations like the data rate of acoustic systems and unstable channel gain have motivated researchers to figure out a better system of underwater visible light communication (UVLC). The UVLC system is able to transmit high data rates up to Gbps [1]. There are significant

applications for underwater communications such as pollution measurement, underwater exploration, maritime archaeology, field exploration for oil, and port security.

There are many studies on the impact of scattering and absorption of light in different types of water with respect to small/large particles, humic/falvic acid, and chlorophyll concentration [2–5]. In [6–8], the authors applied channel modeling in different types of water using the Beer–Lambert law, assuming no objects and utilizing an ideal laser source. Monte Carlo photon tracing has been investigated using an ideal laser source with no human objects [9,10]. In [11], the Haltrin and Kattawar model has been used to consider the impact of absorption and scattering inside sea water, harbors, and coastal water. Arnon *et al.* have studied several scenarios in UVLC: the line-of-sight link, modulating retroreflector link, and reflective link. Furthermore, they provide the required data rate and perform bit error rate (BER) analysis using a green light source [6].

The results obtained in [6,12] motivated us to apply MATLAB simulations and evaluate the best wavelength that can be recommended in sea water in non-line of sight (NLoS) scenarios.

Unlike [2–6], Uysal *et al.* carried out a static channel modeling and characterization study, taking into account the presence of manmade objects for the static environment [13]. Additionally, they used an advanced ray-tracing program, Zemax Optics Studio [14], and used super-blue LED for transmission as well as the reflection characteristics of the water, which are wavelength dependent. In [15], statistical studies of fading in underwater wireless optical channels in the presence of air bubbles and salinity random variations have been applied.

The results in [9–11,16,17] motivated us to add advanced human CAD objects for realistic channel modeling and evaluate the optimum transmitter that can be used in sea water, as the absence of divers and blockage may vary the results dramatically. Additionally, the results in [13] motivated us to use the Zemax Optics Studio and to add the dynamic motion for human CAD objects via using Zemax programming language (ZPL) [18]. The results in [15,19,20] motivated us to perform statistical analysis in the dynamic UVLC similar to that of the underwater free-space optics channel.

In this paper, we first obtain the channel impulse response (CIR) for static scenarios between two divers, where both source and receiver divers are fixed. We carry out a comprehensive study for the average delay and delay spread for different source colors in sea water. We select the best wavelength that has a maximum channel gain in multiple scenarios. In addition, we study the impact of changing the detector area.

In fair agreement with [6], we use the same configuration for static channel modeling in Zemax to obtain the CIR. However, we focus in this section on the best color that can operate properly in sea water. After that, the change of detector area is considered.

In [21], Miramirkhani *et al.* configured a mobile user moving in a trajectory path and obtained the CIR for each movement point. However, they did not obtain the distributions that provide the maximum likelihood for the acquired data, which is highly needed for BER analysis. The results in [21] motivated us to use the practical setup Monte Carlo ray-tracing

(MCRT) simulator, add the dynamic mobility in UVLC, and evaluate the distributions, which offer a goodness of fit for the channel gain variations. They also offer a solution for low-performance results appearing because of severe fading caused by the dynamic channel due to diver movement, blockage, and receiver orientations.

Gong *et al.* assumed strong correlations between detectors in a single-input multiple-output (SIMO) model using ultraviolet radiation in free-space optics [22]. They also studied the effect of temperature, humidity, and wind speed in the absence of human CADs. In our work, we consider no correlation between receivers in the SIMO model, as we focus on dynamic channel modeling, and this assumption will not affect the obtained distributions that depend on severe fading, which affects the received power in the dynamic channel.

In [23], closed-form expressions of BER, capacity, and outage probability of the underwater wireless optical communication system are explained, taking into consideration the effect of scattering, absorption, and misalignment.

Furthermore, we first obtain different statistics for several dynamic scenarios after applying a mobility algorithm using ZPL in two configurations: single-input single-output (SISO) and SIMO.

The remainder of the paper is organized as follows: Section 2 explains the mathematical models used in NLoS communication links. In Section 3, we apply our case studies to reach the optimum results for the best transmitter in sea water in terms of maximum depth and different viewing and receiving angles based on the mathematical models. Section 4 illustrates the CIR for different scenarios using Zemax Optics Studio for static channels. In Section 5, dynamic channel modeling is introduced for four scenarios using a cyan transmitter, and the output is the resulted distributions that match the acquired data. Section 6 is devoted to the main conclusions of this work.

2. NLoS COMMUNICATION LINK

In this section, we illustrate the mathematical models for NLoS scenarios in sea water. We compare the performance of the four colors—cyan, blue, royal blue, and green—inside sea water and then apply the BER performance analysis.

Using the simple expression of total attenuation according to Hartlin’s model, the extinction coefficient $c(\lambda)$ is the sum of the absorption $a(\lambda)$ and the scattering $b(\lambda)$ [3]. So,

$$c(\lambda) = a(\lambda) + b(\lambda). \tag{1}$$

One can derive the link budget for the sensor-to-sensor link as follows: use the variables defined in Eq. (1) and express the auxiliary function for NLoS communication as [6]

$$f_{\text{Aux}} = \eta_T \eta_R e^{(-c(\lambda) \left[\frac{H+x}{\cos(\theta_r)} \right])}, \tag{2}$$

$$g_{\text{Aux}} = \frac{1}{2} \times \left[\left[\frac{\tan(\theta_r - \theta_t)}{\tan(\theta_r + \theta_t)} \right]^2 + \left[\frac{\sin(\theta_r - \theta_t)}{\tan(\theta_r + \theta_t)} \right]^2 \right], \tag{3}$$

$$f_{\text{Rec}} = \frac{P_T \cos(\theta)}{A_{\text{ann}}} \begin{cases} f_{\text{Aux}} \cdot g_{\text{Aux}}, & \theta_{\min} \leq \theta \leq \theta_c \\ f_{\text{Aux}}, & \theta_c \leq \theta \leq \theta_{\max} \end{cases}, \tag{4}$$

where H is the transmitter depth, x is the receiver depth, θ_r is the angle of transmission, and A_{ann} is the illuminated annular surface area of the sphere of radius $(H + x)$ expressed as [6]

$$A_{\text{ann}} = 2\pi(H + x)^2 \times (\cos(\theta_{\min}) - \cos(\theta_{\max})). \quad (5)$$

This yields the approximate received power as

$$P_{\text{NLoS}} \approx A_R \times f_{\text{Rec}}. \quad (6)$$

Substituting Eq. (2) in Eq. (6) and specifically operating in the region where $\theta_c \leq \theta \leq \theta_{\max}$ yields

$$P_{\text{NLoS}} \approx A_R \times \eta_T \eta_R e^{-c(\lambda) \left[\frac{H+x}{\cos(\theta_r)} \right]}. \quad (7)$$

1. BER Performance Analysis

The BER response at different data rate transmissions for OOK NRZ modulation has been investigated. We also compare the maximum depth for the NLoS reflective communication link model through different wavelengths at BER of 10^{-10} . The BER is defined as [6]

$$\text{BER} = \frac{1}{2} \times \text{erfc} \left[\frac{(r_1 T - r_0 T)}{\sqrt{2} (\sqrt{r_1 T} + \sqrt{r_0 T})} \right], \quad (8)$$

where r_0 and r_1 are given as

$$r_0 = r_d + r_{\text{bg}}, \quad (9)$$

$$r_1 = r_d + r_{\text{bg}} + r_s. \quad (10)$$

Here, r_d and r_{bg} represent the sources of the additive noise due to dark counts and background illumination, respectively. The parameter r_s is the photon arrival rate during the gated receiver slot of duration t and is given by [6]

$$r_s = \frac{1}{t} \times \left(\frac{P_R}{R_D} \right) \times \frac{\eta_D}{h\nu}, \quad (11)$$

where R_D is the data rate, η_D is the detector counting efficiency, P_R is P_{NLoS} as defined in Eq. (7), h is the Planck's constant, and ν is the photon frequency. The overall BER is obtained by substituting Eqs. (7), (9), and (10), and Eq. (11) in [Eq. (8)]:

$$\text{BER} = \frac{1}{2} \text{erfc} \left[\frac{\left(r_d + r_{\text{bg}} + \left(\frac{1}{t} \left(\frac{A_R \times f_{\text{Aux}}}{R_D} \right) \frac{\eta_D}{h\nu} \right) \right) T - (r_d + r_{\text{bg}}) T}{\sqrt{2} (\sqrt{(r_d + r_{\text{bg}} + r_s) T} + \sqrt{(r_d + r_{\text{bg}}) T})} \right]. \quad (12)$$

3. CHLOROPHYLL-BASED MODEL PERFORMANCE ANALYSIS IN NLoS SCENARIO

Here, we illustrate the proposed system, with respect to a chlorophyll-based model showing the extinction coefficient values in sea water [6]. Four wavelengths—cyan, blue, royal blue, and green—will be investigated, as they have low extinction coefficients in sea water for absorption and scattering characteristics. The wavelengths of cyan, blue, royal blue, and green are 490 nm, 460 nm, 470 nm, and 532 nm, respectively.

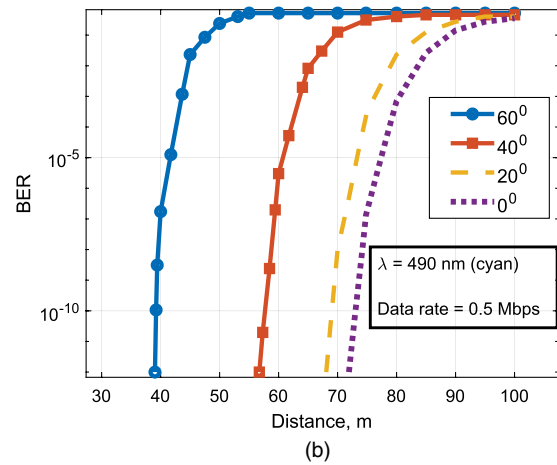
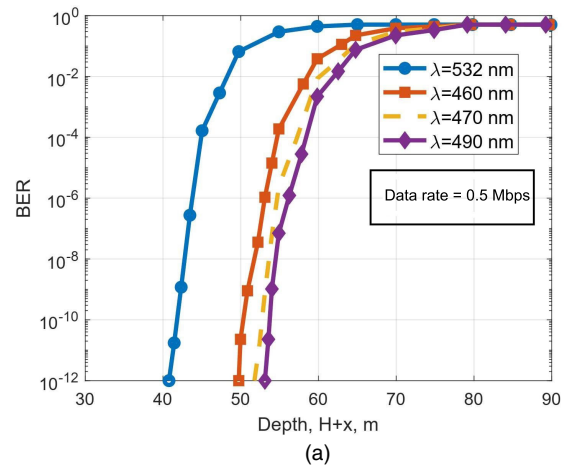


Fig. 1. (a) BER versus depth at 0.5 Mbps and (b) BER versus distance at different viewing angles.

The NLoS communication link includes reflections for the sea surface. BER measurements are illustrated in this subsection. Figures 1–3 are presented by adjusting the suitable parameters using Eq. (12).

Figure 1(a) shows that cyan reaches a deeper depth, ensuring that this is the best wavelength. The receiver position is then taken into consideration within the viewing angle of the

transmitter using the cyan color, as shown in Fig. 1(b), at a data rate of 0.5 Mbps. Clearly, the 0° value shows the best results, and increasing the angle results in a decrease in BER.

As shown in Figs. 2 and 3, the increase in data rate limits the receiving depth. The receiver's angle with respect to the distributed transmitter viewing angle above the critical angle is investigated, as illustrated in Fig. 4. It is noted that the increase in receiving angle limits the depth reached by the receiver. The

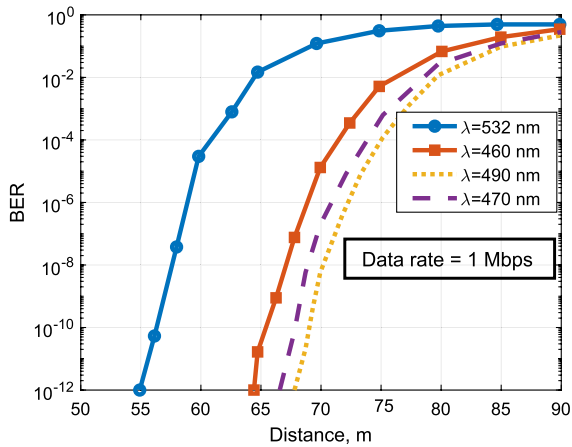


Fig. 2. BER versus depth at data rate 1 Mbps.

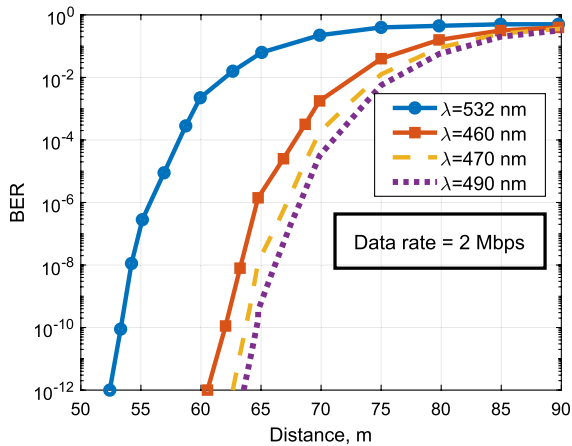


Fig. 3. BER versus depth at data rate 2 Mbps.

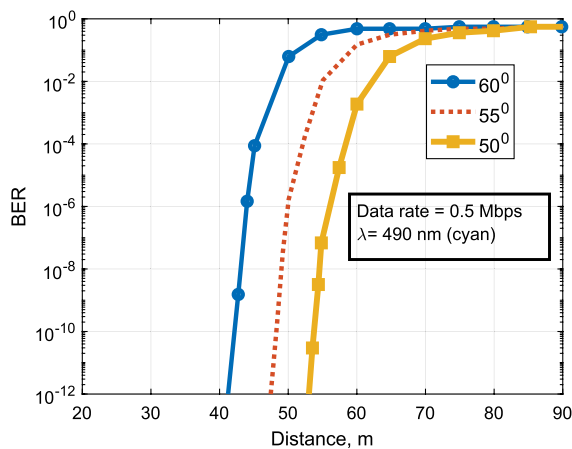


Fig. 4. BER versus depth at different receiving angles.

cyan performance has the lowest absorption and scattering coefficients. Accordingly, the numerical simulation shows that cyan reaches a deeper depth in sea water.

4. STATIC CHANNEL MODELING USING ZEMAX OPTICS STUDIO

In this section, a MCRT simulation is applied using the Zemax Optics Studio program. We obtain the CIR for different scenarios according to the steps shown in Fig. 5. The static model in this section indicates that both the transmitting and receiving divers are fixed in their positions, and they are totally aligned together, as shown in Fig. 6 [13].

In addition, we consider both the Lambertian model and the purely diffuse material, which is considered the worst scenario compared with specular reflections.

The CIR used in the MCRT solver is given by [14]

$$h(t) = \sum_{i=1}^{N_r} p_i \delta(t - \tau_i), \tag{13}$$

where p_i and τ_i are the power and delay for the i th ray, respectively, and N_r is the total number of rays emitted by the LEDs.

The channel DC gain is considered one of the most important parameters needed in VLC channel modeling, which is the output of the Zemax Optics Studio program. We also obtain the CIR for two scenarios: in the first scenario, we compare the four colors in four and 16 LED chips of a circular array. After proving that cyan exhibits the best performance using Zemax Optics Studio, we check the impact of changing the detector area in the second case.

The rms delay spread, τ_{rms} , is widely used to quantify the degree of dispersion of the time of samples compared to the average delay spread τ_0 in the multipath channels. It is defined as the square root of the second central moment of the CIR as follows [13]:

$$\tau_{rms} = \sqrt{\int_0^\infty (t - \tau_0)^2 h(t) dt / \int_0^\infty h(t) dt}. \tag{14}$$

A. Channel Impulse Response

The major steps to obtain the CIR are shown in Fig. 5. First, we specify the geometry of the underwater environment, the objects, the reflection characteristics of surface materials, and the specifications of both light sources and detectors. Then, we use the UVLC channel modeling in Zemax. We use a non-sequential ray-tracing feature of Zemax to calculate the detected power by tracing the rays. Rays that have more than three reflections and do not reach the detector are discarded by the program. In the last step, we import this data to MATLAB

Table 1. Simulation Parameters Used in Zemax Solver

Transmitter specifications	Power: 2 W Cree [13,24]
Receiver specifications	Viewing angle: 120° [24] Aperture area: 5 cm ² [13] Field of view: 180° [13]
Link range (m), depth (m)	25 [13]
Number of rays per LED chip	500,000 rays [24]
Source	Circular array, radius 1 cm

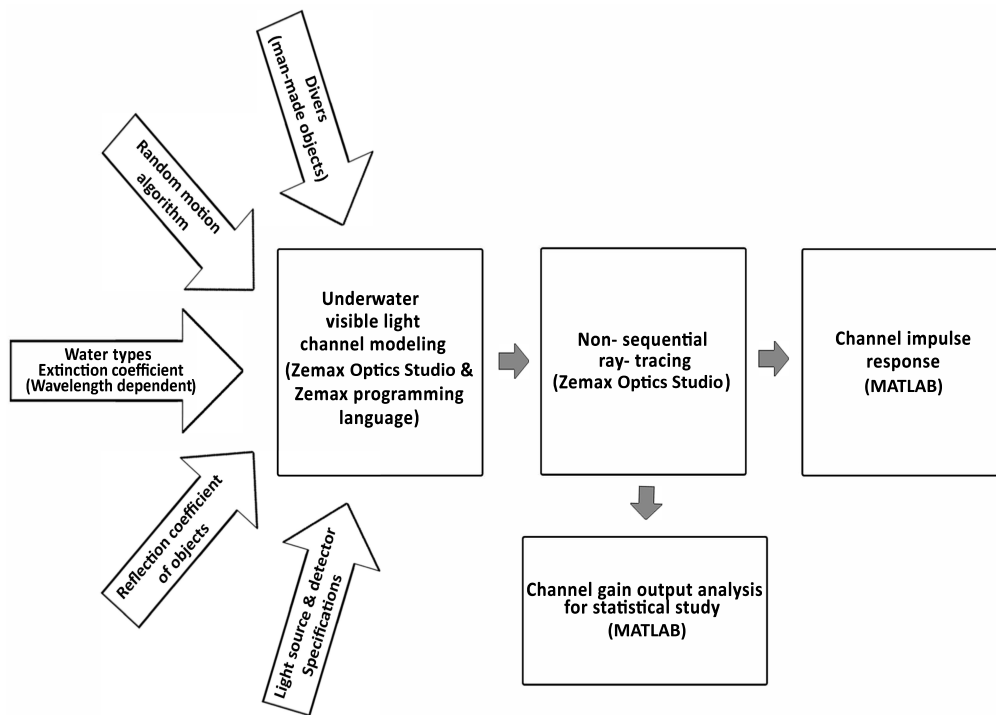


Fig. 5. Steps used in the simulation for dynamic channel modeling and CIR.

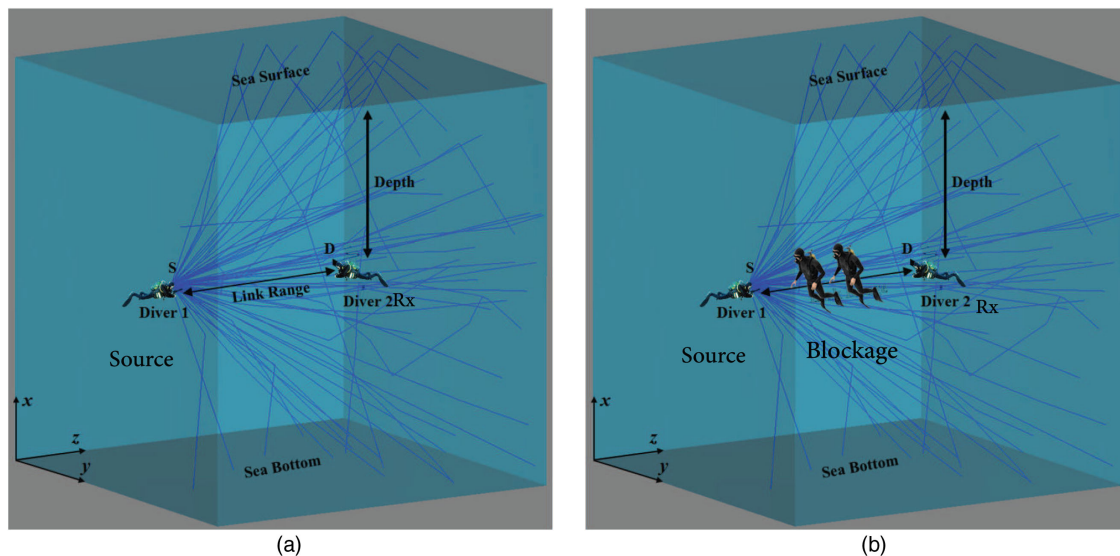


Fig. 6. Aligned SISO communication link for a static environment with and without blockage.

and obtain the CIR. Then, we investigate the best transmitter results in a circular array of different numbers of LED chips and investigate the effect of changing the detector area using the best transmitter. We use the parameters in Table 1 and utilize advanced human CADs [25] with dimensions 1.8 m, 0.4 m, and 0.2 m for height, width, and depth, respectively. As for the source, we use the practical transmitter cree model [26]. Moreover, we add divers as a blockage between the source and receiver divers for realistic simulations, as shown in Fig. 6(b). As shown in Tables 2 and 3, the Zemax simulation results are

exactly the same for royal blue and blue. This is because their extinction coefficients are nearly equal.

1. Case 1: Transmitter Performance in a Circular Array of Four LED and 16 LED Chips

As shown in Fig. 7(a), the received power of cyan exceeds the blue color by 6% and is more than double the performance of the green color. The rms delay of the green color exhibits the lowest values due to the lowest number of rays reaching the detector. The rays of the green color are terminated earlier

Table 2. Circular Array Four LEDs, Radius 1 cm

Transmitter Type	Absorbed Rays	Mean Delay (ns)	RMS Delay (ns)	Received Power (μW)
490 nm (cyan)	13	71.77555	1.850603	1.79
460 nm (blue)	11	71.75348	1.737698	1.63
470 nm (royal blue)	11	71.75348	1.737698	1.63
532 nm (green)	8	71.68917	0.7062054	0.809

Table 3. Circular Array 16 LEDs, Radius 1 cm

Cases	Absorbed Rays	Mean Delay (ns)	RMS Delay (ns)	Received Power (μW)
490 nm (cyan)	34	71.84546	1.773781	5.33
460 nm (blue)	33	71.77176	1.646314	4.85
470 nm (royal blue)	33	71.77176	1.646314	4.85
532 nm (green)	32	71.81093	0.9006616	2.46

Table 4. Circular Array 16 LEDs Cyan LED, Radius 1 cm for Different Detector Areas

Detector Area	Absorbed Rays	Mean Delay (ns)	RMS Delay (ns)	Received Power (μW)
10 cm^2	320	71.77602	2.45126	31.79
7.5 cm^2	43	71.7605	2.327232	6.69
5 cm^2	34	71.84546	1.773781	5.33

than blue and cyan. Table 2 illustrates the mean delay and rms delay and the number of absorbed hits reaching the detector. The same procedure is performed by increasing the circular array LED chips from four LEDs to 16 LEDs and still the cyan exhibits the best performance in terms of channel gain, as shown in Table 3 and Fig. 7(b).

2. Case 2: Cyan Performance in a Circular Array of 16 LEDs for Different Detector Areas

Now simulation is carried out throughout cyan, as we are concerned about the impact of changing detector areas. As expected, the higher the detector area, the more absorbed rays reach the detector. The channel gain performance for the detector area of 7.5 cm^2 increases by an amount of 1.36 μW compared to the 5 cm^2 detector area. Also, increasing the detector area to 10 cm^2 has a dramatic result, and the received power increases by 25.1 μW compared to the 7.5 cm^2 detector area and exceeds the detector area of 5 cm^2 by 26.46 μW . The average delay remains constant in most of the cases, as illustrated in Fig. 8. However, in terms of rms delay, the detector area of 5 cm^2 exhibits the lowest rms delay, as the lowest number of rays reaches the detector. The output results are summarized in Table 4.

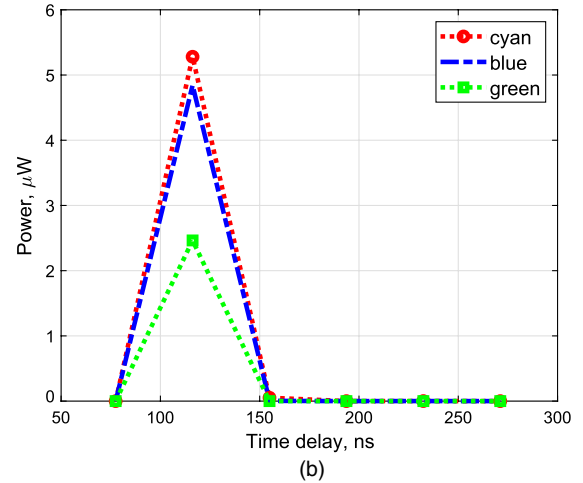
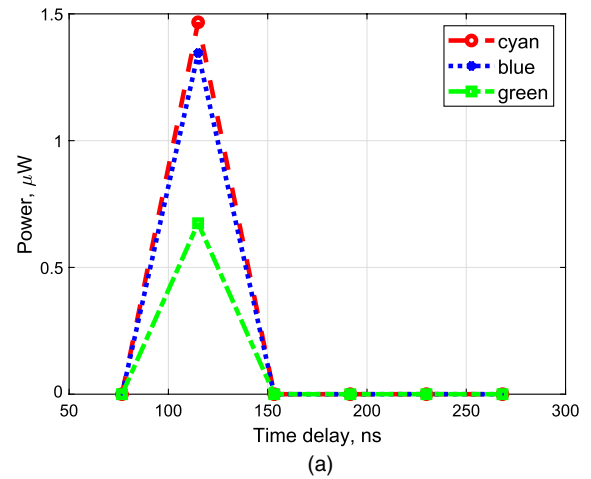


Fig. 7. (a) Circular array radius = 1 cm and N = 4 chips for three different colors in sea water; (b) circular array radius = 1 cm and N = 16 chips for three different colors in sea water.

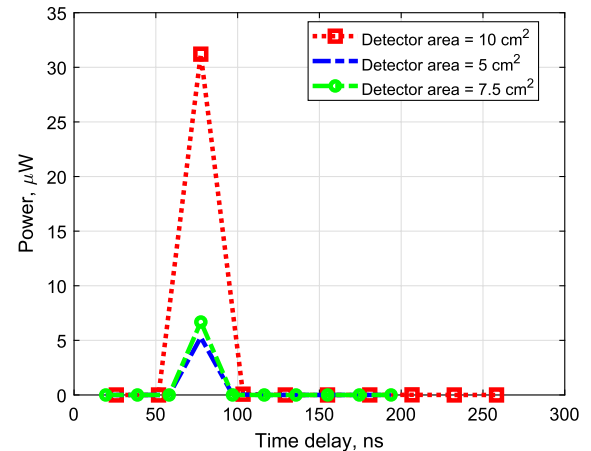


Fig. 8. CIR for circular array 16 LEDs. Source is cyan LED, radius 1 cm for different detector areas.

5. DYNAMIC CHANNEL MODELING USING ZEMAX PROGRAMMING LANGUAGE AND ZEMAX OPTICS STUDIO

The simulation of the static optical wireless channel explores the effects of the VLC channel assuming fixed receivers and transmitters [13]. The static VLC channel depends on definite scenarios and does not include all the possible variations of the channel. Most of the literature discusses the static scenario and does not cover all the possible multi-path and shadowing scenarios. Also, the probability density function (PDF) or cumulative density function (CDF) of the optical received power is not provided. The dynamic channel modeling is a challenging issue that affects communication links and needs to be well investigated [27]. Also, the receiver orientation has a wide field of interest in indoor VLC and can change the channel gain dramatically [28]. In this section, we will study the effect

of fading resulted by the random motion of divers and detector orientation. The sea water extinction coefficient is considered wavelength dependent, as it takes into consideration the effect of scattering. In addition, both scattering and severe fading are considered. The aim of applying this dynamic scenario is to figure out the proper source and detector specifications that can tolerate dynamic channel variations. The output of ZPL is the statistical distributions that can match the received power variations. The aim of applying this dynamic scenario is to figure out the proper source and detector specifications that can tolerate dynamic channel variations. The output of ZPL is the statistical distributions that can match the received power variations. The distribution fit toolbox in MATLAB is used to represent the data using maximum likelihood estimation, and the resulted log likelihood parameter enables to identify the rank of the distributions that can fit the data [29]. The greater the log likelihood number, the more distributions that can fit the data.

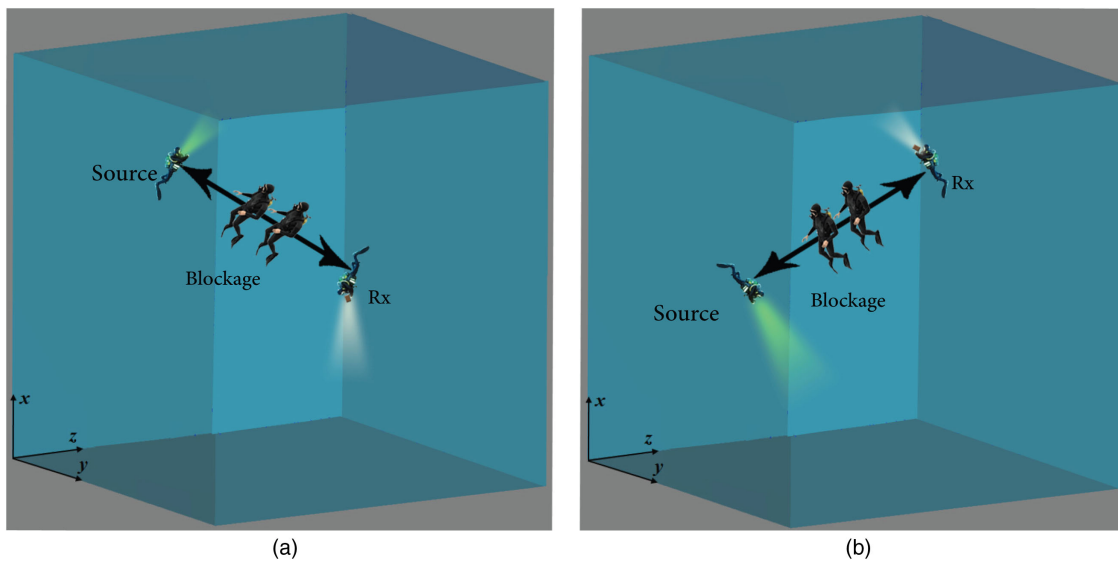


Fig. 9. SISO dynamic model: two divers communicating within dynamic environment in different positions for 400 s.

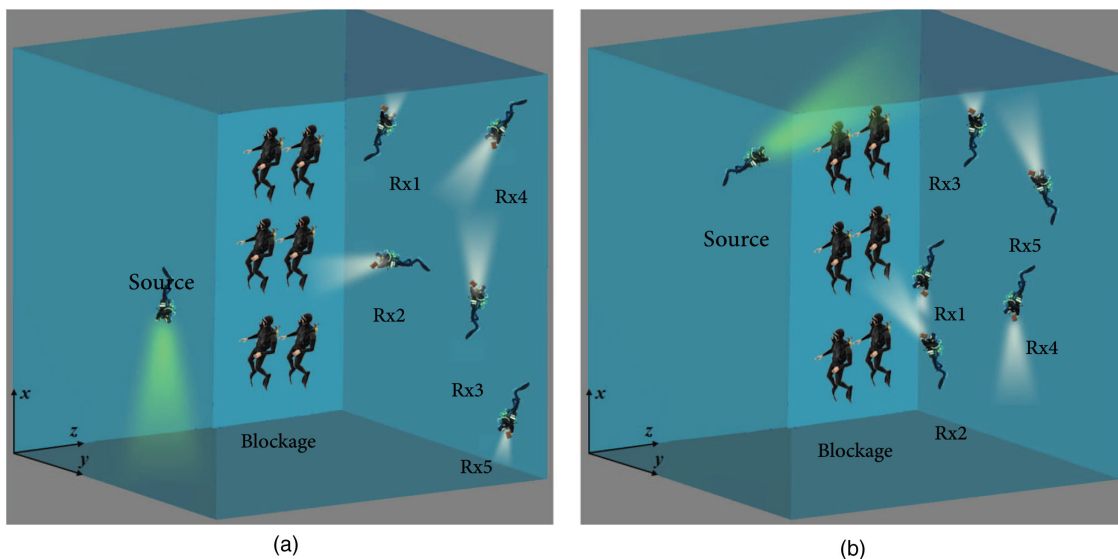


Fig. 10. SIMO dynamic model: transmitting diver is communicating with five divers, each carrying a detector; all divers are moving for 400 s.

A. SISO and SIMO Model Mobility Algorithm

The SISO dynamic model is described as shown in Fig. 9. The path length between the source and receiving divers is configured to be fixed at 23 m. The orientation angle is assumed to be fixed, which means that the divers do not rotate around x axis. The tilt angle is set as a uniform distribution from 0° to 180° . As shown in Fig. 9(a), the tilting angle of the source diver is 25° , and the tilting angle of the receiver diver is 160° . In Fig. 9(b), the dynamic random motion changes the tilting angle of the source diver to 130° , and the receiver diver is changed to 20° . Furthermore, the divers are not aligned in the same horizontal axis as static scenarios, as they can move to any random position in an area of 25 m^2 . Accordingly, the source and receivers have variable x and y coordinates in each simulation and fixed z coordinates. The mobility algorithm in the SIMO scenario is similar to the SISO scenario. The difference is that the source diver communicates with five moving divers, each carrying a detector, as shown in Fig. 10, so the power is shared to five divers instead of one diver. The distance between the transmitting diver and the five receiving divers is fixed, where each diver carrying the receiver is 1.5 m apart. Also, the existence of blockage divers is applied for both SIMO and SISO models for realistic channel modeling. The source beam direction is highlighted with green color, and the receiver beam angle is highlighted with the white color, as illustrated in Figs. 9 and 10.

B. Case 1: SISO Model Using Cyan 4×4 Rectangular Array and a 5 cm^2 Detector Area

We apply the mentioned mobility algorithm for 400 s to get all possible received power variations. The simulation of divers is shown for the SISO model in Fig. 9 using a cyan 4×4 rectangular array, and both divers carrying the source and receiver are moving in a random motion manner. The performance of the channel dc gain is not good, and some readings over the 400 iterations reach zero output due to non-alignment, and many reflected rays do not reach the detector. As shown in Fig. 11(a), the simulation results show that the exponential distribution is the most suitable distribution that can fit the received power. The results motivated us to fetch out a new solution and increase the transmitted power using more chips. The exponential distribution indicates the poor performance of the channel, as noted in Refs. [15,19,30]. The exponential PDF is given as [15]

$$y = f(b|\mu) = \frac{1}{\mu} e^{-\frac{b}{\mu}}, \tag{15}$$

where the resulted distribution parameters are the mean $\mu = 3.78 \times 10^{-6}$, and b is the channel gain.

C. Case 2: SISO Model Using Cyan 10×10 Rectangular Array and a 5 cm^2 Detector Area

The results in the previous case motivated us to increase the array size and use a cyan rectangular array of 10×10 LED chips, as used in [20] and filtered to cyan color only. The performance of the distributions is compared using the log likelihood parameter, which indicates the degree of correlation of the distribution and the channel gain data. The higher the log likelihood number, the better the accuracy of the distribution.

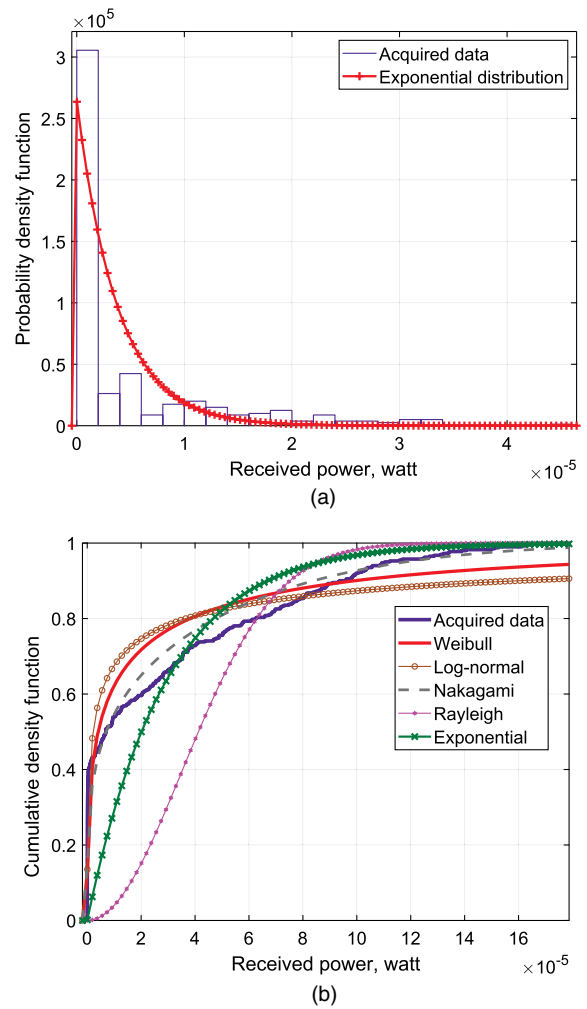


Fig. 11. (a) PDF against received power for the dynamic channel for two divers in SISO model using cyan rectangular 4×4 array and 5 cm^2 detector area; (b) CDF against received power for the dynamic channel for two divers in SISO model using cyan rectangular 10×10 array and 5 cm^2 detector area.

As shown in Fig. 11(b), the results reveal that the Nakagami channel has the maximum log likelihood number with 4229.48, followed by Weibull distribution and log-normal distribution, having 4194.6 and 4175, respectively. The performance of the system is far more enhanced than the previous case using a small array source, and the zero readings disappear. The obtained log-normal distribution is valid for our model, similar to the log-normal turbulence model used in [23], in the performance analysis. In our work, we consider Nakagami distribution, as it exhibits the best performance for representing the data. Accordingly, we consider the Nakagami distribution. The PDF of Nakagami distribution is given by [31]

$$p_m(h_m) = \left(\frac{m}{\Omega}\right)^m \frac{2}{\Gamma(m)} h_m^{2m-1} \exp\left(-\frac{mh_m^2}{\Omega}\right), \tag{16}$$

and the resulted parameters of the distribution are $m = 0.12594$, $\Omega = 2.45508 \times 10^{-9}$.

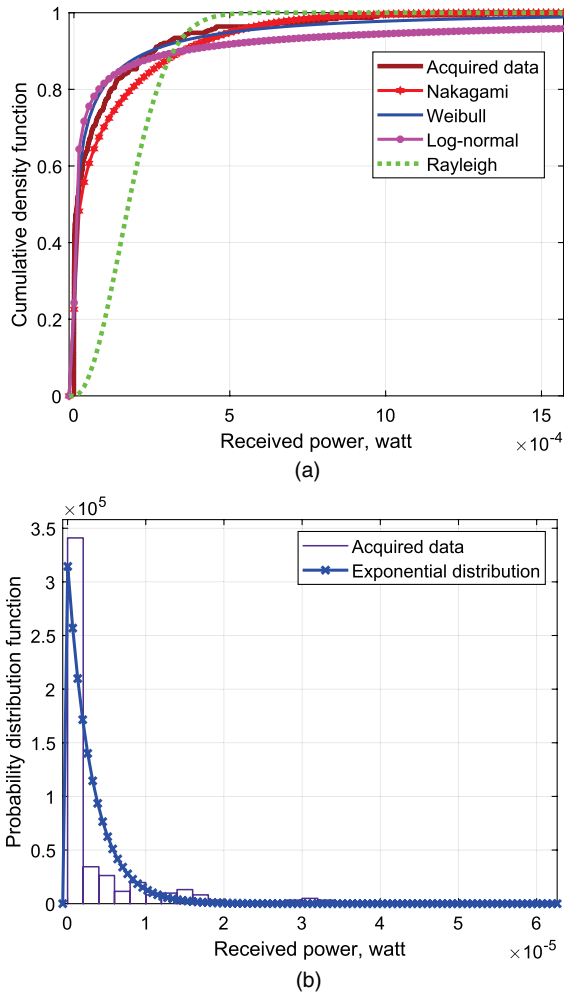


Fig. 12. (a) CDF against received power for the dynamic channel in SIMO model using cyan rectangular 10×10 array and detector 5 cm^2 area; (b) PDF against received power for the dynamic channel in SIMO model using cyan rectangular 10×10 array and detector 1 cm^2 area.

D. Case 3: SIMO Model Using Cyan 10×10 Rectangular Array and a 5 cm^2 Detector Area

Now, we test the successful system appeared in case (SISO model using 10×10 and detector area 5 cm^2) in a more advanced scenario for the SIMO system to check its reliability. The measured detector area for the five receiving divers is still 5 cm^2 , and the output is still similar to the previous. As shown in Fig. 12(a), the results reveal that the Weibull channel shows the maximum log likelihood number of 2940.87, followed by log-normal and Nakagami, having 2934.7 and 2927.5, respectively. The Weibull PDF is given by [31]

$$f(h|a, b) = \frac{b}{a} \left(\frac{h}{a}\right)^{b-1} e^{-(h/a)^b}, \quad (17)$$

where b is the channel gain. The fitting parameters are: shape parameter $b = 0.359$ and scale parameter $a = 2.40129 \times 10^{-5}$.

E. Case 4: SIMO Model Using Cyan 10×10 Rectangular Array and a 1 cm^2 Detector Area

Now we use a detector area of 1 cm^2 as recommended in indoor VLC [20]. The reliability of the system in a small detector area of 1 cm^2 is tested in Zemax, and the results reveal very poor performance and 30% total blockage. The best distribution that can describe the data is the exponential distribution as shown in Fig. 12(b) with a mean of $\mu = 3.161 \times 10^{-6}$.

6. CONCLUSION

In this paper, we provide MATLAB simulations for a NLoS scenario for four common wavelengths: cyan, blue, royal blue, and green. The simulation has been implemented to figure out the effect of changing the viewing angle and receiving angle in sea water. We have also applied a comprehensive practical setup using Zemax in both static and dynamic scenarios. We obtained the CIR for two divers in a static model and applied a dynamic mobility algorithm for the divers using cyan color and obtained statistical distributions that represent the channel gain variations for SISO and SIMO models. The MCRT simulations were carried out in a blockage environment to maintain the worst scenario and assuming purely diffuse materials, and the sea water was configured as wavelength dependent.

In the NLoS link, the cyan color reached the maximum depth of 53 m at a data rate of 0.5 Mbps. The best transmitter viewing angle is at 0° , and as long as the angle increases, the BER decreases. Moreover, the increase in the data rate limits the receiving depth. Additionally, the study of the receiving angles reveals that increasing the receiving angle limits the depth reached by the receiver. As for the CIR, the obtained results using a circular array with different numbers of LED chips prove that the cyan exceeds the blue by 8% and is more than double the performance of the green color. The cyan color is used to obtain the CIR for different detector areas. The received power for the 7.5 cm^2 detector area exceeds the 5 cm^2 area by 20%, and the 10 cm^2 detector area exceeds the 7.5 cm^2 area by 88%. The simulation results for the dynamic model show that the exponential distribution fits the received power data, which exhibits very poor performance and has extremely low power. The fitting parameters for the exponential distribution are mean $\mu = 3.78 \times 10^{-6}$ for the SISO model using a cyan 4×4 rectangular array. After using more chips in a 10×10 array in the SISO scenario, the received power is enhanced. The resulted parameters of Nakagami distribution are $m = 0.12594$ and $\Omega = 2.45508 \times 10^{-9}$, which can fit the received power variations in this case. Also, we recommend using a 10×10 cyan rectangular array and 5 cm^2 detector area in the SIMO model, and the Weibull distribution can fit the data with parameters $a = 2.40129 \times 10^{-5}$ and $b = 0.3594$. Decreasing the detector area in the SIMO scenario to 1 cm^2 leads to an exponential distribution with parameter $\mu = 3.161 \times 10^{-6}$ due to the poor quality of the received signal for the 400 s interval.

Accordingly, the results reveal that using a cyan 10×10 rectangular array and 5 cm^2 detector area can accommodate the dynamic channel variations inside sea water in both SISO and SIMO models. On the other hand, using a cyan 4×4 rectangular array or utilizing a detector area of 1 cm^2 results in extremely

low performance results, and data cannot be demodulated in the receiver for either the SISO or SIMO scenario.

The obtained CDFs due to the dynamic channel gain variations enable the system designers to quantify the effects of divers' motions. These CDFs are also beneficial in designing handover, channel assignment algorithms and high-speed communications using suitable modulation techniques. Also, researchers can use the obtained distributions for localization purposes.

REFERENCES

- Z. Zeng, S. Fu, H. Zhang, Y. Dong, and J. Cheng, "A survey of underwater optical wireless communications," *IEEE Commun. Surv. Tuts.* **19**, 204–238 (2017).
- S. Sathyendranath, "Inherent optical properties of natural seawater," *Defence Sci. J.* **34**, 1–18 (1984).
- V. I. Haltrin, "Chlorophyll-based model of seawater optical properties," *Appl. Opt.* **38**, 6826–6832 (1999).
- O. V. Kopelevich, "Small-parametric model of the optical properties of seawater," in *Ocean Optics I: Physical Ocean Optics* (1983), pp. 208–234.
- V. I. Khalturnin, "Propagation of light in sea depth," in *Optical Remote Sensing of the Sea and the Influence of the Atmosphere*, V. A. Urdenko and G. Zimmermann, eds. (German Democratic Republic Academy of Sciences Institute for Space Research, 1985), pp. 20–62.
- S. Arnon and D. Kedar, "Non-line-of-sight underwater optical wireless communication network," *J. Opt. Soc. Am. A* **26**, 530–539 (2009).
- T. Hamza, M.-A. Khalighi, S. Bourennane, P. Léon, and J. Opederbecke, "Investigation of solar noise impact on the performance of underwater wireless optical communication links," *Opt. Express* **24**, 25832–25845 (2016).
- C. Wang, H.-Y. Yu, and Y.-J. Zhu, "A long distance underwater visible light communication system with single photon avalanche diode," *IEEE Photon. J.* **8**, 1–11 (2016).
- J. Li, Y. Ma, Q. Zhou, B. Zhou, and H. Wang, "Monte Carlo study on pulse response of underwater optical channel," *Opt. Eng.* **51**, 066001 (2012).
- C. Gabriel, M.-A. Khalighi, S. Bourennane, P. Léon, and V. Rigaud, "Monte-Carlo-based channel characterization for underwater optical communication systems," *J. Opt. Commun. Netw.* **5**, 1–12 (2013).
- W. Liu, D. Zou, P. Wang, Z. Xu, and L. Yang, "Wavelength dependent channel characterization for underwater optical wireless communications," in *IEEE International Conference on Signal Processing, Communications and Computing (ICSPCC)* (IEEE, 2014), pp. 895–899.
- S. Arnon, "Underwater optical wireless communication network," *Opt. Eng.* **49**, 015001 (2010).
- F. Miramirkhani and M. Uysal, "Visible light communication channel modeling for underwater environments with blocking and shadowing," *IEEE Access* **6**, 1082–1090 (2017).
- "Zemax 18 release 1, radiant zemax llc," 2018, <https://www.radiantzemax.com/zemax>.
- M. V. Jamali, A. Mirani, A. Parsay, B. Abolhassani, P. Nabavi, A. Chizari, P. Khorramshahi, S. Abdollahramezani, and J. A. Salehi, "Statistical studies of fading in underwater wireless optical channels in the presence of air bubble, temperature, and salinity random variations," *IEEE Trans. Commun.* **66**, 4706–4723 (2018).
- V. Guerra, C. Quintana, J. Rufo, J. Rabadan, and R. Perez-Jimenez, "Parallelization of a Monte Carlo ray tracing algorithm for channel modelling in underwater wireless optical communications," *Procedia Technol.* **7**, 11–19 (2013).
- V. Guerra, O. El-Asmar, C. Suarez-Rodriguez, R. Perez-Jimenez, and J. Luna-Rivera, "Statistical study of the channel parameters in underwater wireless optical links," in *3rd IEEE International Work-Conference on Bioinspired Intelligence (IEEE, 2014)*, pp. 124–127.
- "Zemax programming language," 2018, <https://customers.zemax.com/os/resources/learn/knowledgebase/what-is-zpl>.
- F. D. Ricardo and A. Barrios, "Exponentiated weibull fading model for free-space optical links with partially coherent beams under aperture averaging," *Opt. Eng.* **52**, 1–9 (2013).
- R. Barrios and F. Dios, "Exponentiated weibull model for the irradiance probability density function of a laser beam propagating through atmospheric turbulence," *Opt. Laser Technol.* **45**, 13–20 (2013).
- F. Miramirkhani, O. Narmanlioglu, M. Uysal, and E. Panayirci, "A mobile channel model for VLC and application to adaptive system design," *IEEE Commun. Lett.* **21**, 1035–1038 (2017).
- C. Gong, B. Huang, and Z. Xu, "Correlation and outage probability of NLOS SIMO optical wireless scattering communication channels under turbulence," *J. Opt. Commun. Netw.* **8**, 928–937 (2016).
- P. Saxena and M. R. Bhatnagar, "A simplified form of beam spread function in underwater wireless optical communication and its applications," *IEEE Access* **7**, 105298 (2019).
- F. Miramirkhani and M. Uysal, "Channel modeling and characterization for visible light communications," *IEEE Photon. J.* **7**, 1–16 (2015).
- "Grab CAD models," 2018, <https://grabcad.com>.
- "Cree LEDs," 2018, <http://www.cree.com>.
- S. Dimitrov, R. Mesleh, H. Haas, M. Cappitelli, M. Olbert, and E. Bassow, "On the air of a cellular infrared optical wireless system for an aircraft," *IEEE J. Sel. Areas Commun.* **27**, 1623–1638 (2009).
- Y. S. Eroglu, Y. Yapici, and I. Guvenç, "Impact of random receiver orientation on visible light communications channel," *IEEE Trans. Commun.* **67**, 1313–1325 (2019).
- The Mathworks, Inc., *MATLAB and Statistics Toolbox Release 2019b* (2019).
- S. Nadarajah and A. K. Gupta, "On the moments of the exponentiated Weibull distribution," *Comm. Statist. Theory Methods* **34**, 253–256 (2005).
- M. Lei, P. Zhang, H. Haas, and E. Costa, "Performance analysis of an adaptive modulation system over Nakagami-m fading channels," in *Vehicular Technology Conference. IEEE 55th Vehicular Technology Conference. VTC Spring 2002 (Cat. No. 02CH37367)* (2002), Vol. **3**, pp. 1527–1531.